Effects of charge depletion in dusty plasmas

I. Goertz, F. Greiner, A. Piel

IEAP, Christian Albrechts-Universität, D-24098 Kiel, Germany

Introduction

The charging of an isolated dust grain in a collisionless plasma is well described by the orbital motion limited (OML) model. For laboratory plasmas, the dust particles are negatively charged. Once the charge density represented by dust particles becomes comparable to the ion density, the amount of free electrons is dramatically reduced. The increase of the total dust charge is described by the parameter $P = Aa(\mu\mathrm{m})n_d/n_\infty$ [1], with $A = 1\mu\mathrm{m}(4\pi\varepsilon_0 k_B T_e/e^2)$ and a being the dust particle radius. The parameter P can also be written as $P = 4\pi\lambda_{De}^2 a n_d$. In the limit $P \ll 1$, any dust grain can be considered as an isolated particle (Fig. 1a). The dust charge depletion effect can be understood by a model proposed in Ref. [2]. When $P \approx 1$, the cloud potential Φ_c(II) deviates from the ambient plasma potential Φ_p(I) (Fig. 1b). The dust becomes so densely packed that the potential in the neighborhood of the dust particles can no longer approach Φ_p. When dust density n_d increases even further, the potential barrier between the dust particles vanishes and Φ_c(II) approaches the floating potential Φ_f^p(II) of the dust particles (Fig. 1c) and the cloud can now be considered as a *superparticle*.

Experimental Setup

The measurements are performed in a double plasma device of 50 cm diameter and 120 cm length (cf Fig. 2). For the symmetric operation mode of the double plasma device with a negatively biased separating grid, the grid voltage ($U_g = -100$ V), discharge voltage ($U_d = -72$ V) and the discharge current ($I_d = 50$ mA) are kept fixed in each chamber at an argon pressure of 1.6×10^{-2} Pa. This results in a plasma with typical densities of $n_e = n_i \approx 5 \times 10^{14}$ m^{-3}, electron temperature $T_e \approx 1.7$ eV and ion temperature $T_i \approx T_e/10 \ll T_e$. A constant flow of dust is provided by a dust shower of 95 mm diameter, which is agitated by a piezo-stack. The flow rate is adjusted by varying the driver voltage of the piezo-stack. A maximum dust density of $n_d = 4 \times 10^5$cm^{-3} can be achieved. The dust consists

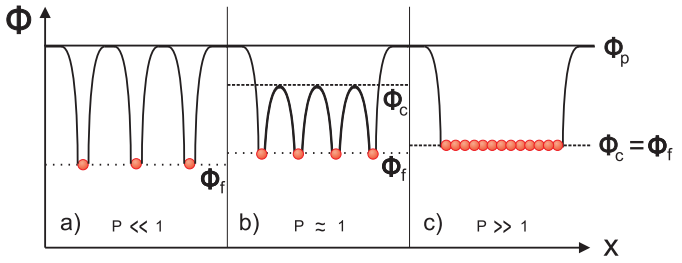

Figure 1: Simplified sketch of the model of Ref. [2]. Φ_p, Φ_c and Φ_f in different regimes of the parameter P.

of monodisperse (5 μm diameter) Alkylsilicon resin SiO_2 particles. The distance between the separating grid and the dust dispenser is 120 mm. The dust densities are measured by laser extinction of a HeNe laser beam ($\lambda = 633$ nm) of intensity $I_0 = 1$ mW. The detected intensity I is given by $I = I_0 \exp\left(-\eta \pi a^2 l n_d\right)$ [3], where $\eta \approx 1$ is the extinction coefficient, l the path length of the laser in the dust cloud, and a the dust particle radius. The dust does not fall down in a cylindrical column but the Coulomb repulsion of the dust particles broadens the dust flow to a cone. Therefore, the actual path length l is measured using the scattered light of a green laser ($\lambda = 532$ nm) that is recorded end-on by a camera.

A three-branch probe arrangement is used to measure the plasma parameters with a plane, a cylindrical, and an emissive probe. The plane probe consists of a 5 mm diameter tantalum disk. The cylindrical probe is a tungsten wire of 0.2 mm diameter and 5mm length. In this experiment both kinds of probes are used for comparability reasons, because shortly after the dust shower is started, the plane probe becomes contaminated, thus the probe is only used in the dust free case. Although contamination is also an issue for the cylindrical probe, the latter can be cleaned by heating the probe wire at electron saturation current. The measurements of plasma and floating potential, however, are made with the emissive probe in two different operating modes, $I_H \approx 1.8$ A (plasma pot. mode) and $I_H \approx 1.0$ A (floating pot. mode). In this way, the emissive probe can also be used to measure the floating potential Φ_f^p with the advantage that the probe can be easily cleaned in the emissive mode. After cleaning, the probe remains uncontaminated for up to 1 s after turning the dust shower on. For measuring the potentials, two positions in the target chamber are chosen: position I in the dust-free-region and position II in the center of the dust shower (Fig. 2). The "dog-leg" probe shaft allows an axial shift and a radial scan by rotating the probe shaft.

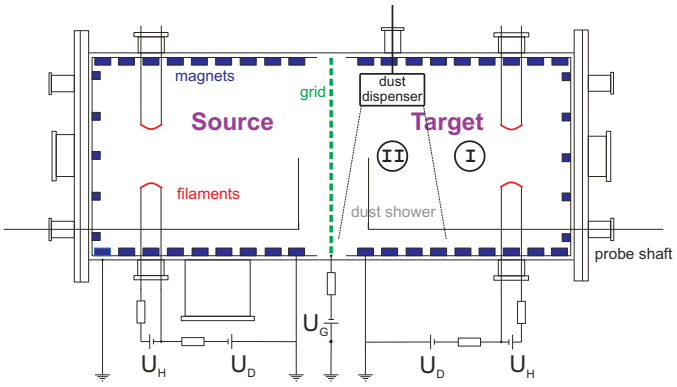

Figure 2: Schematic diagram of the double plasma device with the integrated dust dispenser. I and II mark the positions for the measurements inside and outside the dust shower.

Results

To study dust-depletion effects, it is necessary to measure the cloud potential Φ_c (i.e., the plasma potential inside the dust cloud) and the floating potential Φ_f^p of the probe in the dust shower at position II (Φ_c(II), Φ_f^p(II)) with respect to the plasma potential Φ_p(I) in the ambient dust-free plasma at position I, which may also be affected by introducing a large amount of dust

into the target chamber. Figure 3 presents a set of such measurements for a fixed dust density. The laser extinction signal is shown in panel a) and the intensity reduction corresponds to a dust density of $n_d = 3.5 \times 10^{11}$ m^{-3}. Only one potential profile can be recorded during each dust fall period. Such measurements are shown in Fig. 3b-d. During dust operation, Φ_p(I) breaks down from 2 V to roughly 0 V. The potential in Fig. 3c represents Φ_c(II), which drops from 1.5 V to -2.5 V. The floating potential Φ_f^p(II) given in Fig. 3d increases from -12 V to approximately -10 V. Here, at the starting point of the dust shower, $t = 10$ s, a sharp jump is monitored that is followed by a plateau. After $t = 11$ s, the potential increases during dust shower operation. When the dust shower is turned off ($t = 15$ s), the potentials Φ_p(I) and Φ_c(II) immediately return to their initial values.

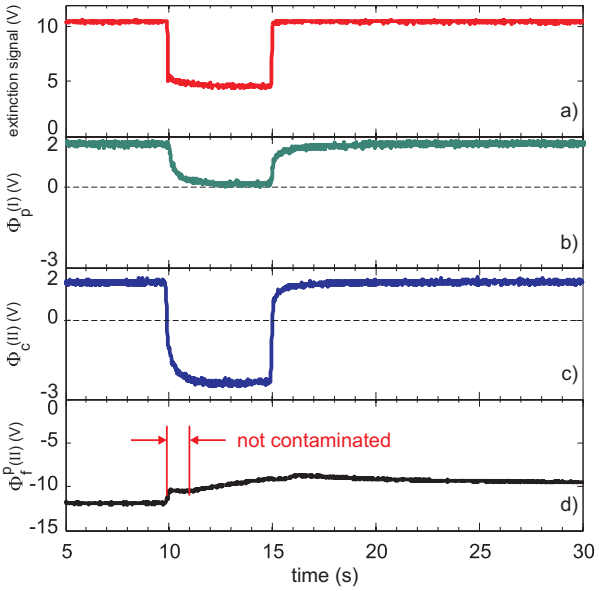

Figure 3: Raw data of the potential measurements. At t = 10 s, the extinction signal a) shows that dust is falling for 5 s. The potentials b) Φ_p(I), c) Φ_c(II) and d) Φ_f^p(II) are measured by the emissive probe.

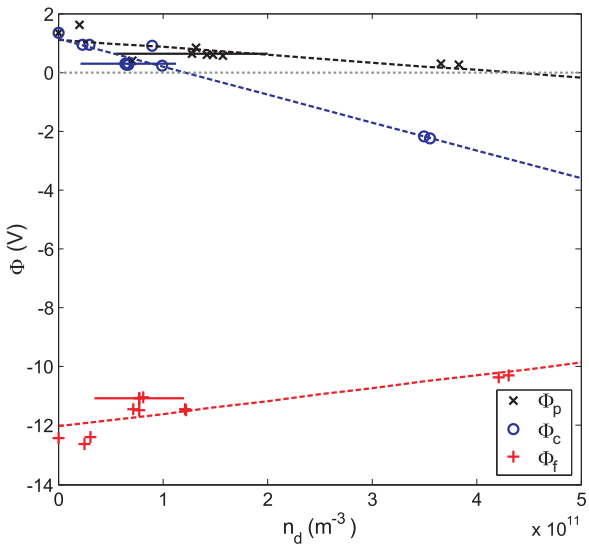

Figure 4: Measured dependence of Φ_p(I), Φ_c(II) and Φ_f^p(II) on dust density n_d

A different behavior is found for Φ_f^p(II), which takes a long time to reach the original value. This effect can be attributed to probe contamination. A consistent set of potential readings Φ_p(I), Φ_c(II), and Φ_f^p(II) is therefore found at $t = 11$ s. Fig. 4 shows the potentials as a function of the measured dust densities in the range of 0.2 to 4.3×10^{11}m^{-3}. The dashed lines in the graph indicate the trends of the data points. When no dust is falling ($n_d = 0$), Φ_p(I) and Φ_c(II) coincide (Φ_p(I) $= \Phi_c$(II) $= 1.34$ V) as expected. The probe floating potential Φ_f^p(II) is at a high negative value (Φ_f^p(II) $= -12.42$ V) due to a group of suprathermal electrons that result from the operation of the filament cathodes. When the dust density increases, both Φ_p(I) and Φ_c(II) decrease, but the slopes differ. The

decrement of Φ_c(II) is stronger than for Φ_p(I). Contrarywise, Φ_f^p(II) increases with n_d, and Φ_c(II) and Φ_f^p(II) are approaching each other. The dashed lines allow an estimate of the change in the potentials at $n_d = 5 \times 10^{11}\mathrm{m}^{-3}$, which corresponds to $P = 3$. These changes are $\Delta\Phi_p(\mathrm{I}) = -1.29$ V, $\Delta\Phi_c(\mathrm{II}) = -4.79$ V, and $\Delta\Phi_f^p(\mathrm{II}) = +2.18$ V. This result shows that significant potential changes occur in the regime $P \lesssim 3$.

Discussion

In summary, we will point out the important observations and conclusions. The observations have shown that the potentials Φ_f^p(II) and Φ_c(II) have to be corrected for the changes in Φ_p(I), so true changes are then $\Delta_{true}\Phi_c(\mathrm{II}) = \Phi_c(\mathrm{II}) - \Phi_p(\mathrm{I}) = -3.5$ V and $\Delta_{true}\Phi_f^p(\mathrm{II}) = \Phi_f^p(\mathrm{II}) - \Phi_p(\mathrm{I}) = -3.47$ V. Therefore, the influence of the dust density on Φ_c(II) and Φ_f^p(II) is verified and allows the following conclusions. Earlier, independent probe measurement in the DP machine have shown that the ion density inside the dust cloud is reduced by recombination on the dust particle (internal wall effect) [3]. This reduces n_e and n_i in the same way but does not affect Φ_f^p(II). We do not assume Φ_f^p(II) to be identical with the surface potential of a dust particle Φ_f^d, rather the influence of charge depletion is captured by the changes of Φ_f^p(II) in the presence of dust, when $n_e < n_i$. The observation of the increased floating potential Φ_f^p(II) justifies the conclusion that $n_e/n_i < 1$. Furthermore the measured decrease of the cloud potential Φ_c(II) below Φ_p(I) is a direct indicator for the dense packing of the dust cloud (so-called Debye overlap). The model, shown in Fig. 1, assumes a constant plasma potential Φ_p(I). The fact that the plasma surrounding the dust shower is also affected by the immersed particles, has to be considered when interpreting the changes of the potentials. The convergence of Φ_f^p(II) and Φ_c(II) shows the effect of electron charge depletion in a dusty plasma. Our achieved results for the potentials in the presence of dust are in line with the model, shown in Fig. 1.

Acknowledgements

We thank Y. Nakamura for hints on the construction of the dust shower. This work was financially supported by DFG under contract SFB-TR24 A2.

References

[1] O. Havnes et al., J. Geophys. Res. A3 **92**, 2281 (1987)

[2] C. K. Goertz, Reviews of Geophysics **27**, 271 (1989)

[3] N. C. Adhikary et al., Physics of Plasmas **14**, 103705, (2007)